

# Numerical iterative approach for zero-order term elimination in off-axis digital holography

Zhonghong Ma,<sup>1</sup> Lijun Deng,<sup>1</sup> Yong Yang,<sup>1,\*</sup> Hongchen Zhai,<sup>1</sup> and Qi Ge<sup>2</sup>

<sup>1</sup>*Institute of Modern Optics, Nankai University, The Key Laboratory of Optical Information Science and Technology of the Education Ministry of China, Tianjin 300071, China*

<sup>2</sup>*College of Zhonghuan Information, Tianjin University of Technology, Tianjin 300071, China*  
\*[yangyong@nankai.edu.cn](mailto:yangyong@nankai.edu.cn)

**Abstract:** A novel numerical iterative approach is proposed to effectively eliminate the zero-order term and to improve the signal-to-noise ratio of the reconstructed image in off-axis digital holography. The iterations are conducted in the spatial domain, resulting in considerable reduction in the computational time and avoiding the subjectivity involved in selecting a filter window in spectral domain. These advantages promote the application of this approach in real-time detection processes. The feasibility of this approach is confirmed by mathematical deductions and numerical simulations, and the robustness of the proposed approach is tested by means of an experimentally obtained hologram.

**OCIS codes:** (090.1995) Digital holography; (100.2000) Digital image processing; (100.3010) Image reconstruction techniques.

---

## References and links

1. E. N. Leith, J. Upatnieks, and K. A. Haines, "Microscopy by wavefront reconstruction," *J. Opt. Soc. Am.* **55**(5), 981–986 (1965).
2. M. Kanka, R. Riesenberger, and H. J. Kreuzer, "Reconstruction of high-resolution holographic microscopic images," *Opt. Lett.* **34**(8), 1162–1164 (2009).
3. Y. Takaki, H. Kawai, and H. Ohzu, "Hybrid holographic microscopy free of conjugate and zero-order images," *Appl. Opt.* **38**(23), 4990–4996 (1999).
4. K. Khare, P. T. S. Ali, and J. Joseph, "Single shot high resolution digital holography," *Opt. Express* **21**(3), 2581–2591 (2013).
5. L. Ma, H. Wang, Y. Li, and H. Jin, "Partition calculation for zero-order and conjugate image removal in digital in-line holography," *Opt. Express* **20**(2), 1805–1815 (2012).
6. I. Yamaguchi and T. Zhang, "Phase-shifting digital holography," *Opt. Lett.* **22**(16), 1268–1270 (1997).
7. I. Yamaguchi, J. Kato, S. Ohta, and J. Mizuno, "Image formation in phase-shifting digital holography and applications to microscopy," *Appl. Opt.* **40**(34), 6177–6186 (2001).
8. P. Guo and A. J. Devaney, "Digital microscopy using phase-shifting digital holography with two reference waves," *Opt. Lett.* **29**(8), 857–859 (2004).
9. N. T. Shaked, Y. Zhu, M. T. Rinehart, and A. Wax, "Two-step-only phase-shifting interferometry with optimized detector bandwidth for microscopy of live cells," *Opt. Express* **17**(18), 15585–15591 (2009).
10. L. Z. Cai, Q. Liu, and X. L. Yang, "Phase-shift extraction and wave-front reconstruction in phase-shifting interferometry with arbitrary phase steps," *Opt. Lett.* **28**(19), 1808–1810 (2003).
11. J. Vargas, J. A. Quiroga, C. O. S. Sorzano, J. C. Estrada, and J. M. Carazo, "Two-step demodulation based on the Gram-Schmidt orthonormalization method," *Opt. Lett.* **37**(3), 443–445 (2012).
12. C. Liu, Y. Li, X. Cheng, Z. Liu, F. Bo, and J. Zhu, "Elimination of zero-order diffraction in digital holography," *Opt. Eng.* **41**(10), 2434–2437 (2002).
13. N. Demoli, J. Mestrovic, and I. Sovic, "Subtraction digital holography," *Appl. Opt.* **42**(5), 798–804 (2003).
14. N. Pavillon, C. S. Seelamantula, J. Kühn, M. Unser, and C. Depeursinge, "Suppression of the zero-order term in off-axis digital holography through nonlinear filtering," *Appl. Opt.* **48**(34), H186–H195 (2009).
15. J. Wu, M. F. Lu, Y. C. Dong, M. Zheng, M. Huang, and Y. N. Wu, "Zero-order noise suppression with various space-shifting manipulations of reconstructed images in digital holography," *Appl. Opt.* **50**(34), H56–H61 (2011).
16. Y. Dong and J. Wu, "Space-shifting digital holography with dc term removal," *Opt. Lett.* **35**(8), 1287–1289 (2010).
17. N. Pavillon, C. Arfire, I. Bergoënd, and C. Depeursinge, "Iterative method for zero-order suppression in off-axis digital holography," *Opt. Express* **18**(15), 15318–15331 (2010).

18. F.B. Souldard, A. Purvis, R. McWilliam, J.J. Cowling, G.L. Williams, J.J. Toriz-Garcia, N.L. Seed, and P.A. Ivey, "Iterative zero-order suppression from an off-axis hologram based on the 2D Hilbert transform", *Biomedical Optics and 3-D Imaging*, OSA Technical Digest (Optical Society of America), paper DSu3C.4.(2012).
  19. J. W. Goodman, *Introduction to Fourier Optics 2nd edition* (McGraw Hill, New York, 1996).
  20. J. P. Liu and T. C. Poon, "Two-step-only quadrature phase-shifting digital holography," *Opt. Lett.* **34**(3), 250–252 (2009).
  21. [http://en.wikipedia.org/wiki/Cosine\\_similarity](http://en.wikipedia.org/wiki/Cosine_similarity)
- 

## 1 Introduction

Off-axis holography [1] has been traditionally used to separate the zero-order image from the two conjugate images, namely, the virtual and real images, from the reconstructed image. Being limited by the fixed pixel size [2] and the number of pixels [3] of the digital recording device, the spectral domain of a hologram, which is common for the zero-order image, and the two conjugate images, is fixed in size. It is necessary to eliminate the zero-order term to enlarge the recordable bandwidth of the sample, thereby improving the quality of the reconstructed complex wave front [4, 5].

Several solutions have been proposed to eliminate the zero-order term in off-axis digital holography. A typical phase-shifting approach in digital holography [6–11] involves the use of a precise vibration-free optical table for successful experimentation [8,9]; further, the time required for recording multi-frame holograms [10,11] renders its application in real-time dynamic processes untenable. A filtering approach has been developed using different types of filters [12–14], where subjective factors significantly influence the selection of the filter window. Moreover, the zero-order term cannot be effectively eliminated using the filtering approach and it has difficulty in coping with the cases when it occurs a big overlap between the zero order term and the real or virtual images. Zero-order term elimination based on various space-shifting manipulations [15, 16] successfully eliminates the zero-order term. However, the reconstructed image is accompanied by several replicas of the original image, which would be a hinder in the improvement of the spatial resolution. Pavillon proposed an iterative method to eliminate the zero-order term [17], wherein the zero-order term of the hologram could be effectively eliminated by performing more than a dozen iterations in the spectral domain. However, performing iterations in the spectral domain is a time-consuming process because of the need of performing Fourier and inverse Fourier transform algorithms during each iteration; further, a suitable filter has to be selected during each iteration. An iterative approach based on the 2D Hilbert transform is proposed by Souldard etc [18], wherein a 2D Hilbert transform are needed in every iteration, which is time consuming due to the included Fourier and inverse Fourier transform. Besides, unless the orientation angle is compensated, the iteration based on 2D Hilbert transform only applies on the retrieval of the object intensity distribution.

In this paper, a novel numerical iterative approach in the spatial domain is proposed to eliminate the zero-order term; in this approach, multi-frame holograms and performing Fourier and inverse Fourier transforms are not required during each iteration. The number of iterations to be performed is also less than that required in the spectral domain; consequently, the time consumed by the proposed approach reduces dramatically. Moreover, the subjectivity involved in selecting a filtering window can be avoided because the same rectangular window is used as a pre-filtering process before the iteration starts, regardless of the content of the hologram. The advantages of the proposed approach are more obvious when a big overlap occurs between the zero order term and the real or virtual image in the Fourier domain. The numerical simulations and experimental results demonstrate the efficiency of the proposed approach in eliminating the zero-order term and improving the quality of the reconstructed image.

## 2 Theoretical analyses

In off-axis digital holography, the intensity of the recorded hologram is denoted as [19]

$$I_H = (\psi_O + \psi_R)(\psi_O + \psi_R)^* = |\psi_R|^2 + |\psi_O|^2 + \psi_O\psi_R^* + \psi_O^*\psi_R, \quad (1)$$

where  $\psi_O$  and  $\psi_R$  denote the object and reference waves, respectively; the asterisk denotes the complex conjugate operator; the last two terms on the right-hand side of Eq. (1) denote the virtual and real images, respectively, while the first two terms on the same side, namely,  $|\psi_O|^2$  and  $|\psi_R|^2$ , should be eliminated to suppress the zero-order image. The amplitude and phase of the reference wave are known for convenient reconstruction; therefore, by subtracting the term  $|\psi_R|^2$  from the hologram representation in Eq. (1) and squaring the result, we get the following.

$$\begin{aligned} (I_H - |\psi_R|^2)^2 &= (|\psi_O|^2 + \psi_O\psi_R^* + \psi_O^*\psi_R)(|\psi_O|^2 + \psi_O\psi_R^* + \psi_O^*\psi_R) \\ &= |\psi_O|^4 + 2|\psi_R|^2|\psi_O|^2 + 2|\psi_O|^2\psi_R^*\psi_O + 2|\psi_O|^2\psi_R\psi_O^* + (\psi_R^*\psi_O)^2 + (\psi_R\psi_O^*)^2 \end{aligned} \quad (2)$$

The initiatory value of the iterative computation of  $|\psi_O|$  is written as  $|\psi_O|_0$ , which can be obtained by using a conventional digital hologram reconstruction method. Substituting  $|\psi_O|_0$  into Eq. (2) and decomposing  $|\psi_O|^4$  into  $|\psi_O|^2|\psi_O|_0^2$ , Eq. (2) can be rewritten in the following form.

$$\begin{aligned} (I_H - |\psi_R|^2)^2 &= |\psi_O|_0^2 \cdot |\psi_O|^2 + 2|\psi_R|^2|\psi_O|_0^2 + 2|\psi_O|_0^2\psi_R^*\psi_O + 2|\psi_O|_0^2\psi_R\psi_O^* \\ &\quad + (\psi_R^*\psi_O)^2 + (\psi_R\psi_O^*)^2 \end{aligned} \quad (3)$$

In the meantime, adding  $|\psi_R|^2$  to the hologram representation in Eq. (1) and multiplying by the initiatory value of the iterative computation  $|\psi_O|_0^2$  yields

$$\begin{aligned} (I_H + |\psi_R|^2) \cdot |\psi_O|_0^2 &= (2|\psi_R|^2 + |\psi_O|^2 + \psi_O\psi_R^* + \psi_O^*\psi_R) \cdot |\psi_O|_0^2 \\ &= |\psi_O|^2|\psi_O|_0^2 + 2|\psi_R|^2|\psi_O|_0^2 + |\psi_O|_0^2\psi_O\psi_R^* + |\psi_O|_0^2\psi_O^*\psi_R \end{aligned} \quad (4)$$

Equations (5) and (6) are obtained by carrying out the Fourier transform of Eqs. (3) and (4), respectively. An off-axis plane wave is used as the reference wave in the proposed approach.

$$\begin{aligned} \mathfrak{F}\{(I_H - |\psi_R|^2)^2\}(u, v) &= \mathfrak{F}\left(|\psi_O|_0^2\right) \otimes G_O(u, v) \otimes G_O^*(u, v) + 2R^2\mathfrak{F}\left(|\psi_O|_0^2\right) \otimes \delta(u, v) \\ &\quad + 2\mathfrak{F}\left(|\psi_O|_0^2\right) \otimes G_O \otimes R\delta(u - u_0, v - v_0) + 2\mathfrak{F}\left(|\psi_O|_0^2\right) \otimes G_O^* \otimes R\delta(u + u_0, v + v_0) \\ &\quad + R^2G_O \otimes G_O \otimes \delta(u - 2u_0, v - 2v_0) + R^2G_O^* \otimes G_O^* \otimes \delta(u + 2u_0, v + 2v_0) \end{aligned} \quad (5)$$

$$\begin{aligned} \mathfrak{F}\{(I_H + |\psi_R|^2) \cdot |\psi_O|_0^2\}(u, v) &= \mathfrak{F}\left(|\psi_O|_0^2\right) \otimes G_O(u, v) \otimes G_O^*(u, v) + 2R^2\mathfrak{F}\left(|\psi_O|_0^2\right) \otimes \delta(u, v) \\ &\quad + \mathfrak{F}\left(|\psi_O|_0^2\right) \otimes G_O \otimes R\delta(u - u_0, v - v_0) + \mathfrak{F}\left(|\psi_O|_0^2\right) \otimes G_O^* \otimes R\delta(u + u_0, v + v_0) \end{aligned} \quad (6)$$

where  $G_O(u, v)$  is the Fourier transformation of the object wave and  $R^2\delta(u, v)$  is the Fourier transformation of the reference intensity, the symbol  $\otimes$  denotes the convolution operation, and  $(u_0, v_0)$  is the spatial carrier frequency of the reference wave.

A rectangular filter with a size equal to one quadrant or two quadrants is used to keep the +1 order, i.e., the third term on the right-hand side of Eqs. (5) and (6), as long as the result of filtering doesn't contain the -1 order spectrum. The filter is fixed in size regardless of the content of the hologram, so the subjectivity in selecting a filter window related to sample is avoided. The results of filtering are expressed using Eqs. (7) and (8), respectively.

$$\begin{aligned} & \Im\{(I_H - |\psi_R|^2)^2\}(u, v) \cdot \text{rect}\left(\frac{u-a/2}{b}, \frac{v-a/2}{b}\right) \\ &= [\Im(|\psi_O|^2) \otimes G_O(u, v) \otimes G_O^*(u, v) + 2R^2 \Im(|\psi_O|^2) \otimes \delta(u, v)] \cdot \text{rect}\left(\frac{u-a/2}{b}, \frac{v-a/2}{b}\right) \quad (7) \\ &+ 2\Im(|\psi_O|^2) \otimes G_O \otimes R \otimes \delta(u-u_0, v-v_0) + R^2 G_O \otimes G_O \otimes \delta(u-2u_0, v-2v_0) \end{aligned}$$

$$\begin{aligned} & \Im\{(I_H + |\psi_R|^2) \cdot |\psi_O|^2\}(u, v) \cdot \text{rect}\left(\frac{u-a/2}{b}, \frac{v-a/2}{b}\right) \\ &= [\Im(|\psi_O|^2) \otimes G_O(u, v) \otimes G_O^*(u, v) + 2R^2 \Im(|\psi_O|^2) \otimes \delta(u, v)] \cdot \text{rect}\left(\frac{u-a/2}{b}, \frac{v-a/2}{b}\right) \quad (8) \\ &+ \Im(|\psi_O|^2) \otimes G_O \otimes R \delta(u-u_0, v-v_0) \end{aligned}$$

Equations (9) and (10) are the inverse Fourier transforms of Eqs. (7) and (8), respectively.

$$\begin{aligned} J_1 &= [|\psi_O|^2 \cdot |\psi_O|^2 + 2|\psi_R|^2 |\psi_O|^2] \otimes [b^2 \sin c(bx, by) \exp(j\pi a(x+y))] \\ &+ 2|\psi_O|^2 \psi_R^* \psi_O + (\psi_R^* \psi_O)^2 \quad (9) \end{aligned}$$

$$\begin{aligned} J_2 &= [|\psi_O|^2 \cdot |\psi_O|^2 + 2|\psi_R|^2 |\psi_O|^2] \otimes [b^2 \sin c(bx, by) \exp(j\pi a(x+y))] \\ &+ |\psi_O|^2 \psi_R^* \psi_O \quad (10) \end{aligned}$$

As the first two terms of Eq. (9) are equal to those of Eq. (10), they can be subtracted; consequently, Eq. (11) is obtained.

$$J_1 - J_2 = |\psi_O|^2 \psi_R^* \psi_O + (\psi_R^* \psi_O)^2 \quad (11)$$

By solving Eq. (11), the solution is shown in Eq. (12).

$$\psi_R^* \psi_O = \frac{-|\psi_O|^2 \pm \sqrt{|\psi_O|^4 + 4(J_1 - J_2)}}{2} \quad (12)$$

Performing the modulo operation on both the sides of Eq. (12) and dividing by  $|\psi_R|$ , the object amplitude can be expressed as follows.

$$|\psi_O| = \left| \frac{-|\psi_O|^2 \pm \sqrt{|\psi_O|^4 + 4(J_1 - J_2)}}{2\psi_R} \right| \quad (13)$$

As evident from Eq. (13), there are two values of  $|\psi_O|$ , namely,

$$|\psi_O|_+ = \left| \frac{-|\psi_O|^2 + \sqrt{|\psi_O|^4 + 4(J_1 - J_2)}}{2\psi_R} \right| \quad \text{and} \quad |\psi_O|_- = \left| \frac{-|\psi_O|^2 - \sqrt{|\psi_O|^4 + 4(J_1 - J_2)}}{2\psi_R} \right|,$$

respectively. Because only one of these values is the closest to the true value, the appropriate value of  $|\psi_O|$  is selected by calculating the relationship between the correlation factor, CF (the level of similarity between the original and reconstructed images), and the intensity ratio,  $A^2$  (the intensity ratio between the reference and object waves [20]).

Here,  $A^2$  can be defined as

$$A^2 = \left| \frac{\psi_R}{\frac{1}{2}[\max(|\psi_O|) + \min(|\psi_O|)]} \right|^2, \quad (14)$$

Further, CF can be defined as

$$CF = \frac{[I_{Re} \star I_{Orig}]_{peak}}{\sum I_{Re}}, \quad (15)$$

where  $I_{Orig}$  and  $I_{Re}$  denote the original object intensity and the reconstructed object intensity, respectively; the symbol  $\star$  denotes the cross-correlation operation. The CF value has different correlations with  $A^2$  when  $|\psi_O|$  in Eq. (13) is either  $|\psi_{O+}$  or  $|\psi_{O-}$ . The  $|\psi_O|$  value that yields a CF value that is the closest to 1 is selected as the new iteration initial value  $|\psi_{O1}|$ . Then, the iteration operation in Eq. (13) is repeated  $(k - 1)$  times, and the final  $|\psi_{Ok}|$  value is obtained. Ultimately, the zero-order term of the hologram is eliminated by substituting  $|\psi_{Ok}|$  into Eq. (1), as shown in Eq. (16).

$$\psi_O \psi_R^* + \psi_O^* \psi_R = I_H - |\psi_O|^2 - |\psi_R|^2 = I_H - (|\psi_{Ok}|)^2 - |\psi_R|^2 \quad (16)$$

### 3 Numerical simulations

The simulation parameters are set as follows: the wavelength of the light source is set as 632.8 nm; the number of pixels is set as 1024 (H)  $\times$  1024 (V) with each individual pixel having a size of 3.75  $\mu\text{m}$   $\times$  3.75  $\mu\text{m}$ . The results of Eq. (13) resulting in “+” and “-” outputs are denoted as  $|\psi_{O+}$  and  $|\psi_{O-}$ , respectively. Here, a simulation using the letter string “NKU” is performed to demonstrate the method for selecting the appropriate sign and to illustrate the convergence of the proposed approach.

The digital hologram (Fig. 1(a)) is constructed using the interference between the string “NKU” and a unit-amplitude plane wave; the corresponding Fourier spectrum is shown in Fig. 1(b). The eventually obtained reconstructed image intensity and the Fourier spectrum of the hologram after zero order suppression are shown in Fig. 1(c) and Fig. 1(d), respectively. A comparison between Fig. 1(b) and Fig. 1(d) reveals that the proposed approach can effectively eliminate the disturbance induced by the zero-order spectrum. The calculated retained zero-order noise through the method presented in reference [17] shows more than 99.8% of the spectral energy of the zero-order term is eliminated.

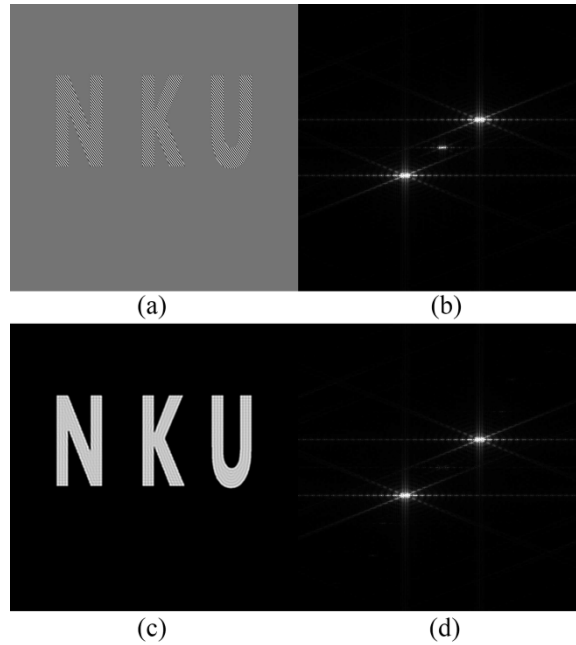


Fig. 1. Simulation of iterative approach. (a) digital hologram; (b) Fourier spectrum of hologram; (c) reconstructed image intensity using proposed approach; (d) Fourier spectrum after eliminating zero-order term.

According to the relationships between the calculated CF and  $A^2$  values, it is reasonable to assume  $|\psi_o|_+$  as  $|\psi_o|$  in the simulation process. Figure 2 shows plots of the relationships between CF and  $A^2$  using  $|\psi_o|$  by assuming  $|\psi_o|_+$  and  $|\psi_o|_-$ . (X-axis represents the  $A^2$  value between the reference and object waves, and Y-axis, the CF value.)

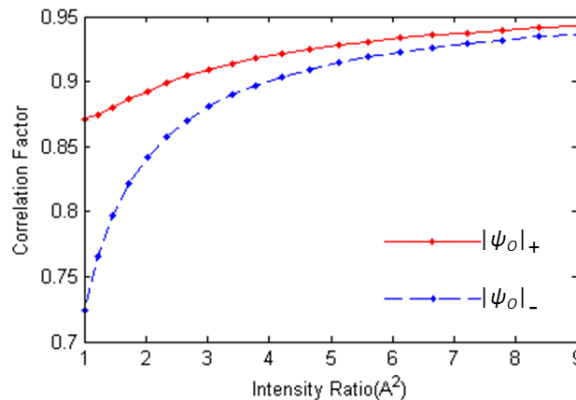


Fig. 2. Relationships between CF and  $A^2$ , where solid line denotes use of  $|\psi_o|_+$  and dashed line, that of  $|\psi_o|_-$ .

From Fig. 2, it is evident that the CF calculated using  $|\psi_o|_+$  is much closer to 1 than that using  $|\psi_o|_-$ . Consequently,  $|\psi_o|$  is assumed to be  $|\psi_o|_+$  in the simulation process. In addition, when  $A^2 = 1$ ,  $CF = 0.87$ , the CF is already above 0.9 when the intensity ratio  $A^2$  reaches to 3. The improvement of CF value is not obvious, even though the intensity ratio further increases. According to the interference theory, the contrast of the interference fringes would decrease as the intensity difference between the object and reference wave increases. Therefore, the intensity ratio  $A^2$  is suggested within the scope that greater than or equal to

1 and less than or equal to 3, considering the environmental noise and vibration in the practical experiment, which would make it difficult in capturing hologram with comparatively low fringe contrast. In the simulation process,  $A^2 = 2$ , and the number of iterations required for reconstruction is 3.

The convergence of the iterative approach is also calculated. From the curve shown in Fig. 3, three iterations are sufficient to suppress the zero-order term for a particular  $A^2$  value. The CF value becomes constant as the number of iterations increases. Simultaneously, it is evident that a larger  $A^2$  value helps to obtain a higher CF value.

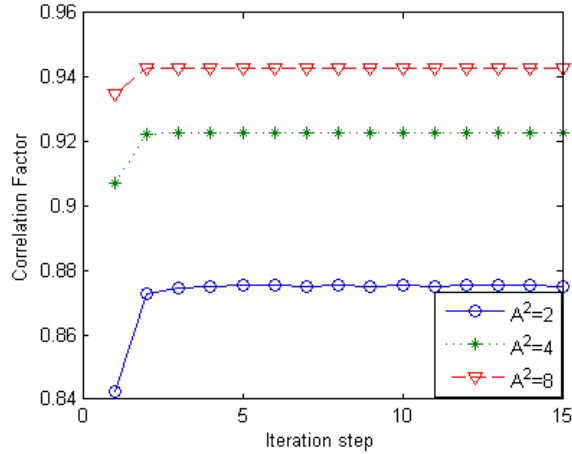


Fig. 3. Correlation factor verses iteration steps for different  $A^2$ .

The following simulations are carried out to compare the quality of the reconstructed images before and after the iteration process under the same conditions of filtering parameters. An image plane hologram of a school badge of the Nankai University ( $A^2 = 1$ ) is shown in Fig. 4(a). The digital hologram is Fourier-transformed into its spectral-domain representation in which the unwanted zero-order spectrum is superimposed on the useful  $\pm 1$ -order spectrum. After three iterations, the zero-order spectrum is eliminated, as shown in Fig. 4(c). The directly reconstructed image from the + 1-order term of Fig. 4(b) contains a group of redundancy fringes resulting from the spectrum of the zero-order term, as shown in Fig. 4(e). By comparison, the redundancy fringes have a lesser influence on the image in Fig. 4(f) reconstructed from the image in Fig. 4(c).

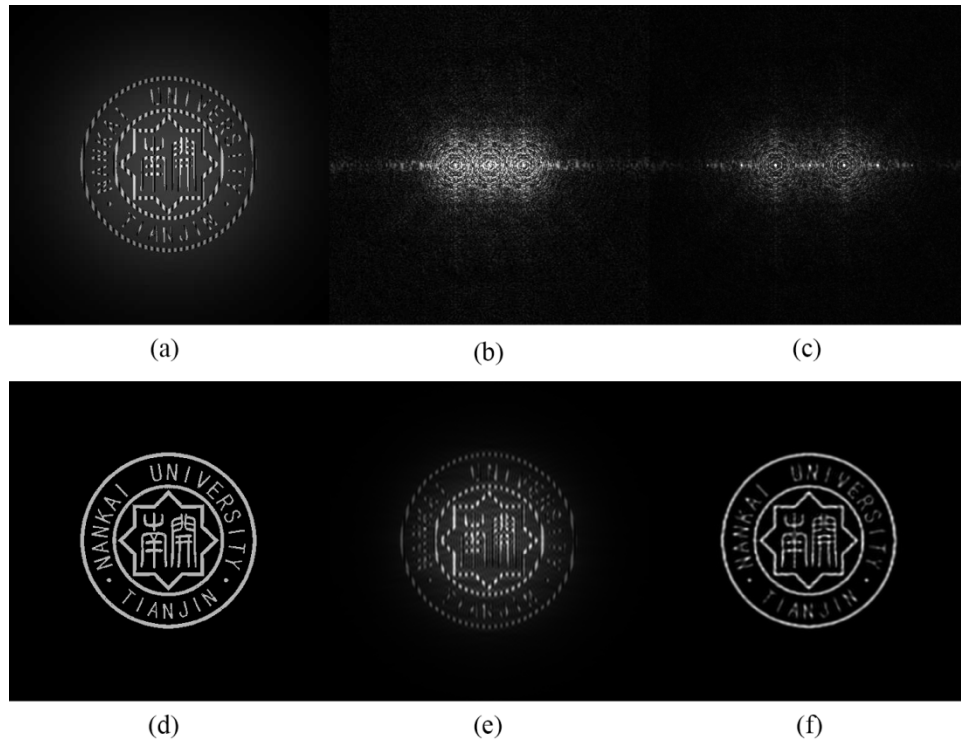


Fig. 4. Simulation results for sample with higher bandwidth. (a) Digital hologram; (b) spectrum of digital hologram in (a); (c) spectrum processed using proposed approach; (d) original object intensity of school badge of Nankai University; (e) reconstructed image from +1-order spectrum of (b); (f) reconstructed image from +1-order spectrum of (c).

Numerical results reveal that the CF value of the image in Fig. 4(f) with the original image is as high as 0.8549 (Fig. 4(d)), whereas the CF value of the directly reconstructed image of Fig. 4(e) with the original image is 0.6466. These results were confirmed by using the cosine similarity analysis [21], which is independent of the image intensity. The cosine similarity calculation requires reshaping the matrixes corresponding to the images in Fig. 4(d), Fig. 4(e), and Fig. 4(f) into one-dimensional vectors. Further, the closer this value is to 1, the more similar the reconstructed image is to the original. The cosine similarity value between Fig. 4(f) and Fig. 4(d) is 0.8645, which is better than that between Fig. 4(e) and Fig. 4(d), i.e., 0.6739. The amount of retained zero-order noise in Fig. 4(c) is 2.79%, indicating that most of the spectral energy carried by the zero-order has been suppressed.

The ability of the iterative approach in reconstructing the phase information is tested using a phase hologram. Since a marginal area is occupied by the zero-order spectrum in the phase-only hologram, the experimentally recorded intensity of a plane wave (Fig. 5(b)) is introduced to modulate the uniform amplitudes of the object and reference waves. The introduced noise in the amplitude results in a relatively large area of the zero-order term; therefore, it is significantly easier to observe the effect of the iterative approach for eliminating the zero-order term.

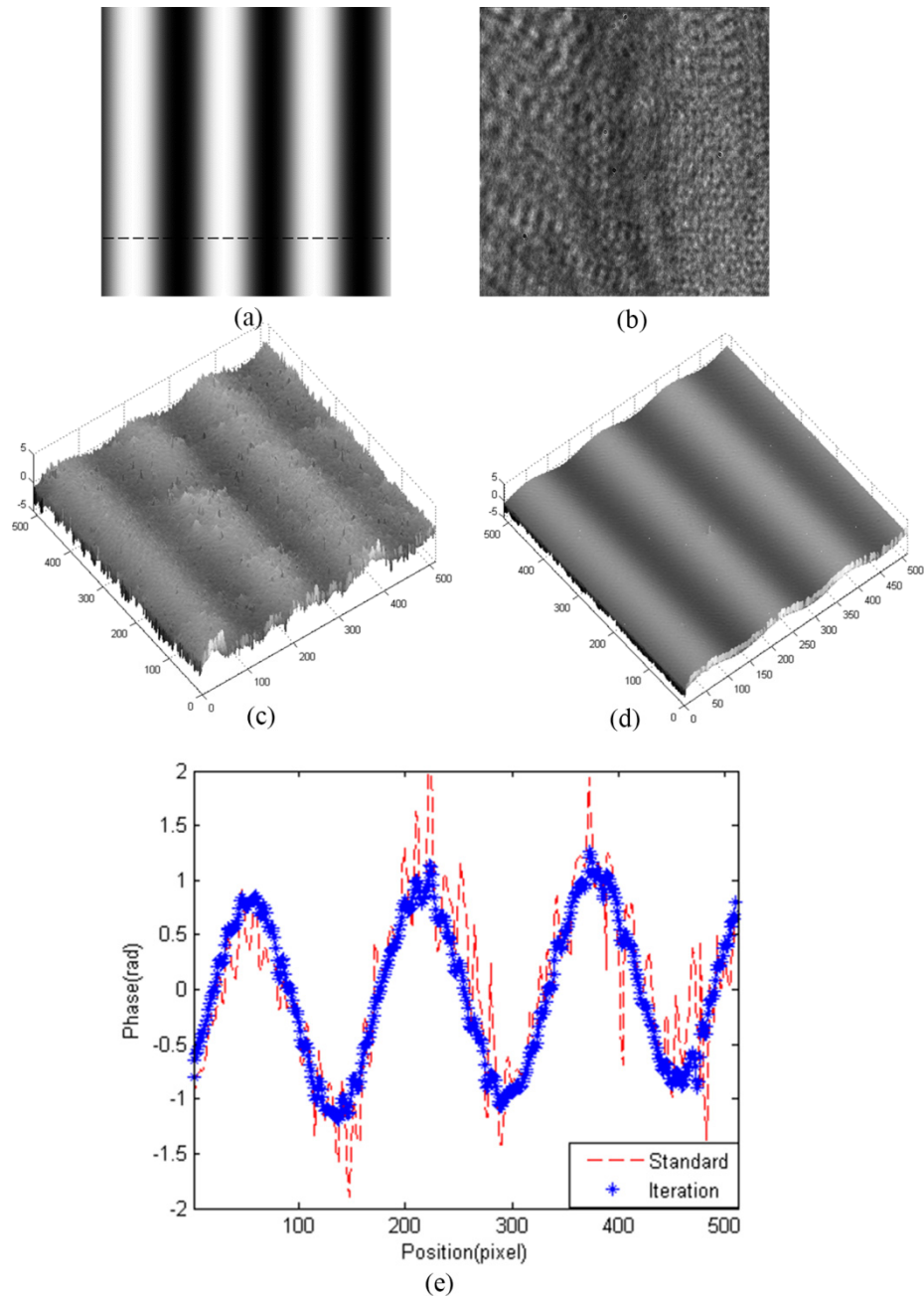


Fig. 5. Phase profile reconstruction. (a) Sinusoidal phase; (b) amplitude information; (c) phase reconstructed using standard approach; (d) phase reconstructed using iterative approach; (e) tomographic phase profile of dashed lines in Fig. 5(a) using standard and iterative approaches.

Figure 5(a) shows the sinusoidal phase (range:  $\pm 1$  rad) used in the simulation, and Fig. 5(b) is the experimentally obtained amplitude information. Here, the phase hologram is formed using  $A^2 = 2$ . The reconstructed phases before and after the iteration processing are shown in Fig. 5(c) and Fig. 5(d), respectively; a reduction in the noise is obvious. The tomographic phase profiles corresponding to the dashed lines shown in Fig. 5(a) for both standard and iterative reconstructions are shown in Fig. 5(e). The curves show that the phase

reconstructed using the iterative approach is closer to the true value of the phase than that obtained using standard reconstruction. A regular sinusoidal curve is distinctly identifiable with regard to the iterative approach, while the sinusoidal curve with regard to the standard approach is significantly distorted because of its strong noise content.

#### 4 Experimental results and analyses

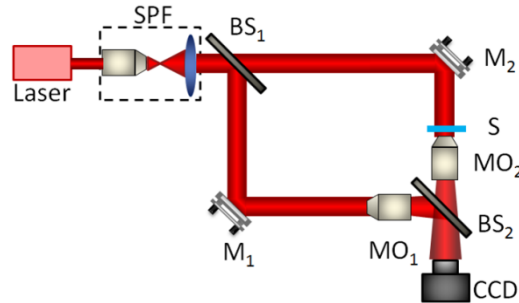


Fig. 6. Schematic diagram of experimental configuration. (SPF: spatial filter; BS: beam splitter; M: mirror; S: sample; MO: microscope objective)

The proposed approach is verified by means of an experiment; the setup is shown in Fig. 6. In this experiment, a 1951 USAF resolution test chart is illuminated with a continuous wave He–Ne laser operating at a wavelength of 632.8 nm. The microscope objectives in both the arms are used to offset the spherical phase. The interference pattern is captured by using a commercially available charge-coupled device (Chameleon CMLN-13S2M, 1280 (H) × 960 (V) pixels with an individual pixel size of  $3.75 \mu\text{m} \times 3.75 \mu\text{m}$ ).

The Fourier spectrum of the experimentally obtained digital hologram is shown in Fig. 7(a). After three iterations, the zero-order term, which induces a disturbance in the  $\pm 1$ -order spectrum, is effectively eliminated, as shown in Fig. 7(b). The signal-to-noise ratio is obviously improved after the zero-order term is eliminated, as evident from the framed rectangular parts in Fig. 7(c) and in Fig. 7(d). The framed rectangular parts at the bottom are the corresponding enlarged parts of the framed parts on the top. It is also evident that the reconstructed image in which the zero-order term is eliminated has more uniform intensity distribution than that of the directly reconstructed one. The CF value between the image in Fig. 7(c) and the original object is 0.8521, while that between the image in Fig. 7(d) and the original one is 0.9249, which reveals a dramatic improvement in the image quality. The amount of retained zero-order noise in Fig. 7(b) is 2.73%, proving the proposed approach to be a high efficiency tool in eliminating the zero-order term.

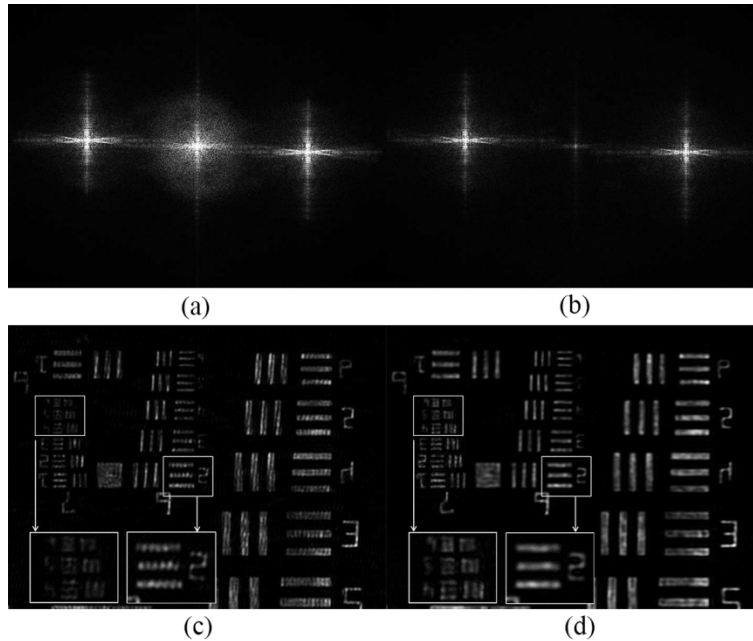


Fig. 7. Output comparison before and after iterative approach processing. (a) Fourier spectrum of directly obtained hologram; (b) Fourier spectrum processed using iterative approach; (c) reconstructed image using spectrum filtering; (d) reconstructed image using iterative approach.

To ensure the effectiveness of the proposed approach, two conditions should be satisfied simultaneously. The first condition is that the intensity distribution of the off-axis plane reference wave is detectable. When record the intensity distribution of the reference wave, the environment should be kept as stable as possible. As a fixed plane wave is generally used as the reference wave, this condition is realizable. The second condition is that the  $+1$  order spectrum and  $-1$  order spectrum are well separated with each other, which can be realized by adjusting the angle between the object wave and the reference wave. In order to make sure the high frequencies to be fully included in the spectral domain, the maximal spectral width of the sample  $\Delta f$  should be within  $66.7\text{mm}^{-1}$  corresponding to the pixel size of the CCD camera of  $3.75\mu\text{m}$ .

## 5 Conclusions

In this paper, a novel numerical iterative approach for effectively eliminating the zero-order term in off-axis digital holography is proposed. The computational time required for the proposed approach has been significantly reduced since the iterations are undertaken in the spatial domain. In addition, only one frame of the hologram obtained from the common experimental setup is sufficient for reconstruction. Hence, the proposed approach is particularly suitable for the real-time detection of a dynamic process in off-axis digital holography. Moreover, the subjectivity introduced in selecting a filter window can be avoided when using the proposed approach. As confirmed by the numerical simulations and experimental results, the proposed approach is proven to be a powerful tool for improving the signal-to-noise ratio of the reconstructed image.

## Acknowledgments

This work is supported by the Special Fund for Basic Research on Scientific Instruments of the National Natural Science Foundation of China (Grant No. 61227010) and the Natural Science Foundation of Tianjin (Grant No.11JCYBJC01400).